PHYSICAL REVIEW VOLUME 97, NUMBER 6 MARCH 15, 1955

Free Magnetic Induction in Nuclear Quadrupole Resonance

M. BLOOM,* *Physics Department, University of Illinois, Urbana, Illinois*

AND

E. L. HAHN AND B. HERZOG, *Watson Scientific Laboratory, Columbia University, New York, New York*

(Received December 14, 1954)

The free precession of an ensemble of nuclear quadrupole moments in an axial electric field gradient is studied by the pulsed nuclear induction method. A quantum-mechanical analysis describes the free precession and spin echo signals which result from the application of single and double pulses of radio-frequency field at the condition of zero-field quadrupole resonance. Beat modulation effects exhibited by free precession signals in a small constant external magnetic field are predicted by analysis. An alternative semiclassical description of quadrupole precession is given, which is analogous to the macroscopic nuclear induction equations of Bloch. Theory is verified by observation of free precession signals of chlorine in $NaClO_3$.

I. INTRODUCTION

RECENTLY the authors published brief reports[1,2] on the discovery of magnetic induction effects due to free nuclear precession in pure quadrupole resonance. These effects follow very closely the spin echo phenomena[3] observed in nuclear moments coupled to a strong externally applied magnetic field. The aim of this paper is to develop the theory needed to explain induction phenomena in quadrupole systems and to describe the basic experiment.

When a system of nuclear spins is placed in a magnetic field H_0 in the usual nuclear induction experiment, the thermal equilibrium established between the spins and their surroundings provides a Boltzmann population distribution among the various spin states. The nuclear ensemble therefore exhibits a nonzero macroscopic magnetization $\mathbf{M}_0$ parallel to H_0. Suppose that $\mathbf{M}_0$ is suddenly rotated to make an angle θ with respect to H_0. $\mathbf{M}_0$ will then precess about H_0 at the Larmor frequency $\omega_0=\gamma H_0$, where γ is the nuclear gyromagnetic ratio. An inductive coil wound about the nuclear sample with its axis perpendicular to H_0 will then, as a result of free nuclear precession, have a voltage induced in it which is proportional to $\omega_0 M_0 \sin\theta$. In practice such a voltage decays in a time T_2, where T_2 is the time taken for different nuclei in the sample to loose precessional coherence because of the following effects: (1) different fixed rates of precession throughout the spin sample volume caused by static internal "local" fields or by an applied inhomogeneous magnetic field; (2) spin lattice relaxation; (3) processes which cause random fluctuation of precessional frequency and phase arising from spin-spin coupling and, particularly in the case of liquids, molecular self-diffusion in an external field gradient.[3]

In the spin echo experiment, free induction signals are observed after transitions have been induced in the spin system by an rf magnetic field, perpendicular to H_0, applied in the form of pulses. If the rf field of magnitude $2H_1$ at a frequency $\omega\approx\omega_0=\gamma H_0$ is applied for a time t_w, the nuclear magnetization vector $\mathbf{M}_0$ is rotated through an angle $\theta=\gamma H_1 t_w$, provided that $t_w \ll T_2$. If pulses are applied at times $t=0$, $t=\tau$, and $t=T$ for example, free induction signals are observed following each of the pulses; and they occur in addition at times $t=2\tau$, $T+\tau$, $2T$, $2T-\tau$, and $2T-2\tau$ as spin echo signals. The properties of free induction signals have facilitated accurate measurements of the spin-lattice relaxation time T_1, the total relaxation time T_2 (or inverse line width), and self-diffusion in gases and liquids in magnetic resonance experiments[3–5] where such measurements would have been very inaccurate or impossible by steady state methods. For a detailed physical model of spin echoes the reader is referred to the literature.[3,6]

In the zero-field nuclear quadrupole resonance experiment,[7,8] an oscillating magnetic field causes transitions between energy levels corresponding to different orientations of the nuclear charge distribution with respect to crystalline electric field gradients. Since the electric interaction is invariant with respect to reversal of the nuclear spin direction, no macroscopic nuclear magnetization is present at thermal equilibrium. It is therefore not obvious that free induction effects similar to spin echo phenomena previously studied can be produced here. From the quantum-mechanical calculation which follows,[9] it will be seen, however, that the effect of inducing magnetic transitions by pulses of the rf magnetic field is to produce a macroscopic oscillating nuclear magnetization. For the case of a symmetric electric field gradient ∇E, this magnetization is produced in the plane perpendicular to the axis of sym-

* Present address: Kammerlingh Onnes Laboratory, University of Leiden, Leiden, The Netherlands.
[1] M. Bloom and R. E. Norberg, Phys. Rev. **93**, 638 (1954).
[2] E. L. Hahn and B. Herzog, Phys. Rev. **93**, 639 (1954).
[3] E. L. Hahn, Phys. Rev. **80**, 580 (1950).
[4] H. Y. Carr and E. M. Purcell, Phys. Rev. **94**, 630 (1954).
[5] D. F. Holcomb and R. E. Norberg, Phys. Rev. (to be published).
[6] E. L. Hahn, Phys. Today **6**, No. 11, 4 (1953).
[7] H. G. Dehmelt and H. Kruger, Z. Physik **129**, 401 (1951).
[8] R. V. Pound, Phys. Rev. **79**, 685 (1950).
[9] A similar quantum-mechanical method for calculating spin echoes is given by E. L. Hahn and D. E. Maxwell, Phys. Rev. **88**, 1070 (1952).

metry of ∇E, and its precessional motion can be given a semiclassical description.

II. THEORY

The electric field gradient tensor $\mathbf{\nabla E}$ is assumed to be symmetric about the z axis. The quadrupole interaction $\mathbf{Q}\cdot\mathbf{\nabla E}$, where $\mathbf{Q}$ is the nuclear quadrupole moment tensor, then satisfies the eigenvalue equation[8]

$$-(\mathbf{Q}\cdot\mathbf{\nabla E})\phi_m=\frac{-e^2qQ}{4I(2I-1)}[3m^2-I(I+1)]\phi_m=E_m\phi_m, \tag{1}$$

where eq is the scalar electric field gradient, eQ is the scalar nuclear electric quadrupole moment, and I is the nuclear spin $(I>\frac{1}{2})$. We choose the representation in which ϕ_m is the eigenfunction of I_z. The matrix elements for the spin operators I_z and $I_\pm=I_x\pm iI_y$ in Dirac notation are then given by

$$\begin{aligned}(m|I_\pm|m\mp1)&=[(I\pm m)(I\mp m+1)]^{\frac{1}{2}},\\(m|I_z|m)&=m.\end{aligned} \tag{2}$$

An rf field $2H_1$ which couples to the nuclear magnetic moment induces transitions corresponding to $\Delta m=\pm1$. Because of the degeneracy of the $\pm m$ states, there are I transition frequencies for integral spin and $I-\frac{1}{2}$ transition frequencies for half-integral spin. When no constant magnetic field is applied, the calculation of induction signals for all transitions are identical except for multiplicative constants. It will therefore be sufficient to treat only the single transition for $I=\frac{3}{2}$ in order to illustrate the general properties of the induction effects.

A. Zero External Magnetic Field Case

The Hamiltonian in this case is given by

$$\mathcal{H}=-\mathbf{Q}\cdot\mathbf{\nabla E}-\gamma\hbar\mathbf{I}\cdot\mathbf{H}(t). \tag{3}$$

The rf coil provides a magnetic field $|\mathbf{H}(t)|=H_x=2H_1\cos\omega t$ along the x axis for $0\leq t\leq t_w$ and $H_x=0$ for $t>t_w$. The wave function ψ for $I=\frac{3}{2}$ is expressed in terms of the eigenfunctions of the electric quadrupole interaction as

$$\psi=\sum_{m=-\frac{3}{2}}^{\frac{3}{2}}C_m(t)\phi_m e^{-i\omega_m t}, \tag{4}$$

where $\omega_m=\omega_{-m}=E_m/\hbar$. We now solve the time-dependent Schrödinger equation,

$$i\hbar\dot{\psi}=\mathcal{H}\psi, \tag{5}$$

in the region $0\leq t\leq t_w$. After substituting (3) and (4) into (5), and using the orthogonality properties of ϕ_m, we obtain

$$\begin{aligned}\dot{C}_m=i\omega_1[&(m|I_+|m-1)e^{i(\omega_m-\omega_{m-1})t}C_{m-1}\\&+(m|I_-|m+1)e^{i(\omega_m-\omega_{m+1})t}C_{m+1}]\cos\omega t,\end{aligned} \tag{6}$$

where $\omega_1=\gamma H_1$. For $I=\frac{3}{2}$, when

$$|\omega-(\omega_{\frac{3}{2}}-\omega_{\frac{1}{2}})|\ll 1/t_w\omega_1,$$

near resonance, Eq. (6) gives

$$\begin{aligned}\dot{C}_{\pm\frac{3}{2}}&=(\sqrt{3}/2)i\omega_1 C_{\pm\frac{1}{2}},\\\dot{C}_{\pm\frac{1}{2}}&=(\sqrt{3}/2)i\omega_1 C_{\pm\frac{3}{2}}+2i\omega_1 C_{\mp\frac{1}{2}}\cos\omega t.\end{aligned} \tag{7}$$

For our experiments, where the conditions $\omega t_w\gg2\pi$ and $\omega_1\ll\omega$ are well satisfied, the term containing $\cos\omega t$ in (7) may be neglected since its contribution to the induction will be vanishingly small. Equations (7) have solutions:

$$\begin{aligned}C_{\pm\frac{3}{2}}(t)&=C_{\pm\frac{3}{2}}(0)\cos(\sqrt{3}\omega_1 t/2)+iC_{\pm\frac{1}{2}}(0)\sin(\sqrt{3}\omega_1 t/2),\\C_{\pm\frac{1}{2}}(t)&=C_{\pm\frac{1}{2}}(0)\cos(\sqrt{3}\omega_1 t/2)+iC_{\pm\frac{3}{2}}(0)\sin(\sqrt{3}\omega_1 t/2).\end{aligned} \tag{8}$$

At $t=0$ the spin system is in thermal equilibrium and an excess spin population is established in the $m=\pm\frac{3}{2}$ states for positive e^2qQ. With the normalization condition that $\sum_m|C_m(t)|^2=1$, and considering the normalization only with respect to the excess population, the initial population coefficients at $t=0$ become

$$C_{\frac{3}{2}}(0)=1/\sqrt{2},\quad C_{-\frac{3}{2}}(0)=e^{i\beta}/\sqrt{2},\quad\text{and}\quad C_{\pm\frac{1}{2}}(0)=0, \tag{9}$$

where β is a random phase factor over which the physical observables must be averaged. This variable expresses the fact that in coming into thermal equilibrium with the lattice the nuclei have interacted with randomly phased electric and magnetic fields.[10] After applying the conditions in (9) to Eqs. (8), the population coefficients after the rf pulse are

$$\begin{aligned}C_{\frac{3}{2}}(t_w)&=(1/\sqrt{2})\cos(\sqrt{3}\omega_1 t_w/2),\\C_{\frac{1}{2}}(t_w)&=(i/\sqrt{2})\sin(\sqrt{3}\omega_1 t_w/2),\\C_{-\frac{3}{2}}(t_w)&=e^{i\beta}C_{\frac{3}{2}}(t_w),\quad C_{-\frac{1}{2}}(t_w)=e^{i\beta}C_{\frac{1}{2}}(t_w).\end{aligned} \tag{10}$$

The solution of the Schrödinger equation (5) during free nuclear precession when $t\geq t_w$ and $H_1=0$ is

$$\psi=\sum_{m=-\frac{3}{2}}^{\frac{3}{2}}\phi_m C_m(t_w)e^{-i\omega_m(t-t_w)}, \tag{11}$$

where expressions for $C_m(t_w)$ are given in (10). The free induction signal will be produced in the xy plane by a nonvanishing nuclear magnetization which is proportional to the expectation value of I_+, expressed as

$$\bar{I}_+=(\psi^*|I_+|\psi)=(\psi^*|I_x|\psi)+i(\psi^*|I_y|\psi). \tag{12}$$

Inserting ψ from (11) into (12) the average values of the operators are found to be

$$\bar{I}_x=(\sqrt{3}/2)\sin\sqrt{3}\omega_1 t_w\sin\omega_0(t-t_w),\quad\bar{I}_y=0,\quad\bar{I}_z=0, \tag{13}$$

where $\omega_0=\omega_{\frac{3}{2}}-\omega_{\frac{1}{2}}=e^2qQ/(2\hbar)$.

[10] R. C. Tolman in *Principles of Statistical Mechanics* (Oxford University Press, London, 1938), p. 351.

A macroscopic oscillating nuclear magnetization proportional to $\bar{I}_x$ is thus set up along the x axis of the rf coil, and it is in fact linearly polarized along this axis. We will show this more clearly in the next section by proving in general that the net magnetization vectors derived from the $+m$ and $-m$ states independently obey quasi-classical differential equations of nuclear induction analogous to those obtained by Bloch.[11] The quantity $\sqrt{3}\omega_1 t_w$ represents the angle θ through which both of the magnetization vectors associated with $+m$ and $-m$ have been rotated by H_1.

As in the case of free precession in a field H_0, different rates of precession for nuclei can cause a dephasing and consequent attenuation of $\bar{I}_x$. This can be introduced phenomenologically in our theory, as was done before,[3] by averaging $\bar{I}_x$ over a distribution of frequencies:

$$g(\omega_0'-\omega_0)=[\exp-(\omega_0'-\omega_0)^2/(2\delta^2)]/(2\pi\delta^2)^{\frac{1}{2}}, \quad (14)$$

where

$$\int_{-\infty}^{\infty} g(\omega_0'-\omega_0)d\omega_0'=1,$$

and δ is the root-mean-square deviation in precessional frequency (relative to an average frequency ω_0) due to a spread in the field gradient eq over the sample volume. Strains and imperfections in the crystal and a temperature gradient over the sample (eq is temperature dependent) will contribute to δ. The effect of magnetic dipolar broadening and of externally applied magnetic fields will be discussed later when a constant magnetic field is introduced into our calculation. With decay now due to an eq variation, neglecting all other relaxation affects, the observed induction for $t\geqslant t_w$ from (13) [let $\omega_0\rightarrow\omega_0+(\omega_0'-\omega_0)$] becomes

$$\begin{aligned}\bar{I}_{x\mathrm{Av}}&=\int_{-\infty}^{\infty} g(\omega_0'-\omega_0)\bar{I}_x d\omega_0'\\ &=(\sqrt{3}/2)\sin\sqrt{3}\omega_1 t_w \sin\omega_0(t-t_w)\\ &\qquad\times\exp[-\delta^2(t-t_w)^2/2]. \quad (15)\end{aligned}$$

When a second pulse of width t_w is applied at $t=2\tau$, an echo is formed, given by

$$\begin{aligned}\bar{I}_{x\mathrm{Av}}=-(\sqrt{3}/2)\sin(\sqrt{3}\omega_1 t_w)\sin^2(\sqrt{3}\omega_1 t_w/2)\sin\omega_0(t-2\tau)\\ \times\exp[-(t-2\tau)^2\delta^2/2], \quad (16)\end{aligned}$$

where $t\geqslant\tau+t_w$. These solutions are similar to those obtained for $I=\frac{1}{2}$ in nuclear magnetic resonance, except that ω_1 in that case is replaced by $\sqrt{3}\omega_1$ here. Equations (15) and (16) apply to the case of a single crystal where all nuclei are oriented by a gradient eq which is perpendicular to the axis of the rf coil. In a powdered crystalline sample, the effective rf component is $H_1\sin\theta_1$ where θ_1 is the angle between H_1 and the axis of spin quantization. The observed component of I_x along the coil axis is $I_x\sin\theta_1$. Introducing these considerations into (15), for example, the observed induction for a powdered sample is then obtained by averaging I_x with respect to θ_1 over a sphere. The integral

$$S=\int_0^{\pi}\sin^2\theta_1\sin(\sqrt{3}\omega_1\sin\theta_1 t_w)d\theta_1$$

is then applied, where S replaces the factor $\sin(\sqrt{3}\omega_1 t_w)$ in (15). The integration gives the summation

$$\begin{aligned}S&=2\sum_0^{\infty}\frac{(-1)^n(2\sqrt{3}\omega_1 t_w)^{2n+1}n!(n+1)!}{(2n+1)!(2n+3)!}\\ &=\frac{8}{3}J_1(\sqrt{3}\omega_1 t_w)-\sum_{n=1}^{\infty}\frac{J_{2n+1}(\sqrt{3}\omega_1 t_w)}{(2n+1)(2n-1)(2n+3)}.\end{aligned}$$

Since this series converges very rapidly, only the first few Bessel functions are of importance. The principle behavior of S is then determined by $J_1(\sqrt{3}\omega_1 t_w)$.

III. QUASI-CLASSICAL NUCLEAR INDUCTION EQUATIONS FOR ZERO FIELD QUADRUPOLE RESONANCE

In this section, we show how a general set of differential equations may be obtained to describe a quasi-classical vector model of the expectation values of nuclear magnetization discussed in the previous section.[12] The procedure in the last section has given the result of this process for $I=\frac{3}{2}$. A vector model of the behavior of the magnetization vectors corresponding to the $+m$ and $-m$ states will now be obtained. This method however does not apply generally in the presence of a constant magnetic field H_0.

Let $a_m(t)=C_m(t)e^{-i\omega_m t}$, and let

$$\psi=\sum_m a_m(t)\phi_m \quad (17)$$

represent the total wave function only for those nuclei which have positive m values. Since there is no mixing between $+$ and $-m$ states when the Hamiltonian (3) is used, it is sufficient to analyze the motion for $+m$ states only. The final result will describe the corresponding $-m$ states also except that they perform a spin precession in a direction opposite to that of the $+m$ states. In the Hamiltonian (3), let

$$\mathbf{I}\cdot\mathbf{H}=(I_+H_-+I_-H_+)/2,$$

where $H_\pm=H_x+iH_y$. Using ψ from (17), the Schrödinger equation (5) provides a differential equation for the population coefficient a_m:

$$\begin{aligned}\dot{a}_m=i\omega_m a_m+(i\gamma/2)\{H_+[(I-m)(I+m-1)]^{\frac{1}{2}}a_{m+1}\\ +H_-[(I+m)(I-m+1)]^{\frac{1}{2}}a_{m-1}\}. \quad (18)\end{aligned}$$

The resonance experiment provides a single rf fre-

[11] F. Bloch, Phys. Rev. **70**, 460 (1946).

[12] A related macroscopic description of quadrupole systems is given by F. Lurçat, Compt. rend. **238**, 1386 (1954).

quency at a quadrupole transition corresponding to $\pm m \rightleftarrows \pm m-1$. Two differential equations are then obtained from (18), one for $\dot{a}_m$ and another for $\dot{a}_{m-1}$ (substitute $m-1$ for m). Terms involving the transitions $m-1 \rightleftarrows m-2$ and $m \rightleftarrows m+1$ may be dropped because the applied rf excites only the $m \rightleftarrows m-1$ transitions. The observed spin angular momenta are given by the following general definitions of expectation values:

$$\bar{I}_z = \sum_m m a_m{}^* a_m; \qquad \bar{I}_\pm = \sum_m (m|I_\pm|m\mp1) a_m{}^* a_{m\mp1}; \tag{19}$$

and their derivatives are given by

$$d\bar{I}_z/dt = \sum_m m(\dot{a}_m{}^* a_m + a_m{}^* \dot{a}_m); \qquad d\bar{I}_\pm/dt = \sum_m (m|I_\pm|m\mp1)(\dot{a}_m{}^* a_{m\mp1} + a_m{}^* \dot{a}_{m\mp1}). \tag{20}$$

Expressions for a_m and a_{m-1} from (18) are substituted into (20). Terms then are collected together in (20) which are the definitions of $\bar{I}_{x,y}$ in (19). The net macroscopic magnetic moment contributed by the m states is defined by $M_{x,y} = \bar{I}_{x,y}\gamma\hbar N$, where N is the total number of spins in the crystal. The net macroscopic z component of magnetism which is involved in the induction will be shown to be defined by

$$M_z = \gamma\hbar N(|a_m|^2 - |a_{m-1}|^2)/2,$$

and is not to be confused with the total magnetization which is proportional to $\bar{I}_z$ in (19). The nuclear induction equations are then

$$\begin{aligned} dM_x/dt &= M_y\omega_0 - \gamma\zeta M_z H_y, \\ dM_y/dt &= \gamma\zeta M_z H_x - M_x\omega_0, \\ dM_z/dt &= \gamma[M_x H_y - M_y H_x], \end{aligned} \tag{21}$$

where $\zeta = (I+m)(I-m+1)$ and ω_0 is the transition frequency. These equations are similar to those obtained by Bloch[11] in describing the behavior of spins in a magnetic field. Following his procedure, a transformation is made to a frame of reference in which the xy plane rotates at the frequency of the applied rf field H_1. Therefore the vector $\mathbf{M}(M_x,M_y,M_z)$ in the laboratory frame transforms to the vector $\mathbf{M}(u,v,M_z)$ in the rotating frame, where H_1 is fixed parallel to the u component. The transformation is given by

$$M_x = u\cos\omega t - v\sin\omega t; \quad M_y = \mp(u\sin\omega t + v\cos\omega t); \quad H_x = H_1\cos\omega t; \quad H_y = \mp H_1\sin\omega t. \tag{22}$$

For positive e^2qQ, looking along the positive z direction, the minus sign is chosen for counterclockwise precession of the magnetization for $+m$, and the plus sign is chosen for clockwise precession of the magnetization for $-m$. Both rotating components of the rf field are therefore utilized in the quadrupole resonance. Applying (22) to the Eqs. (21), the nuclear induction equations in the rotating frame are

$$\begin{aligned} du/dt + (\omega_0-\omega)v &= 0, \\ dv/dt - (\omega_0-\omega)u + (I\pm m)(I\mp m+1)\omega_1 M_z &= 0, \\ dM_z/dt - \omega_1 v &= 0, \end{aligned} \tag{23}$$

where the signs are chosen according to the independent transitions $\pm m \rightleftarrows \pm m-1$. The observed induction due to equal contributions from both signs of m is obtained from (22) as

$$\begin{aligned} \mathfrak{M}_x &= M_x(m) + M_x(-m) = 2(u\cos\omega t - v\sin\omega t), \\ \mathfrak{M}_y &= M_y(m) + M_y(-m) = 0, \\ \mathfrak{M}_z &= M_z(m) + M_z(-m) = 0. \end{aligned} \tag{24}$$

No signal of induction would be detected in a coil oriented at right angles to the rf coil, which serves in our experiment to detect $\mathfrak{M}_x$ as well as transmit $2H_1$. For the case where a single rf pulse is applied, as discussed in the previous section, the induction signal is described by

$$\mathfrak{M}_x = 2[(I+|m|)(I-|m|+1)]^{\frac{1}{2}} M_0 \times \sin[(I+|m|)^{\frac{1}{2}}(I-|m|+1)^{\frac{1}{2}}\omega_1 t_w] \sin\omega_0(t-t_w) \tag{25}$$

upon solving (23), where the net magnetization at thermal equilibrium is

$$M_0 = \gamma\hbar N(|C_{|m|}(0)|^2 - |C_{|m|-1}(0)|^2)/2 \text{ for a given } |m|.$$

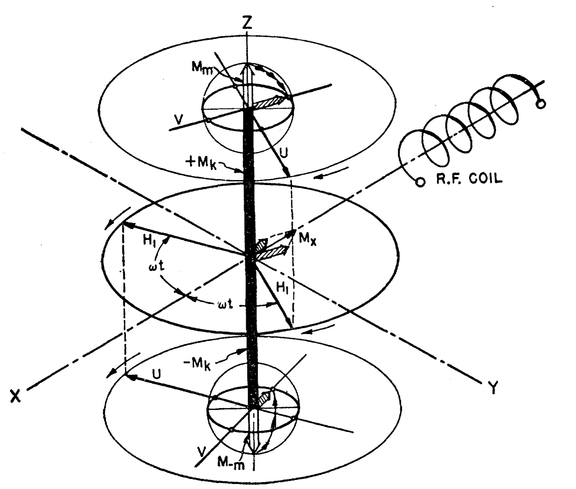

FIG. 1. Vector model of macroscopic spin precession in an axial electric field gradient for positive signs of e^2qQ and γ. The special case is shown where the macroscopic moment vectors $M_{|m|}$ and $M_{-|m|}$ are rotated by 90° about the rf field H_1 during a single pulse. This vector model is not to be taken as a rigorous representation of the motion described by Eqs. (21) during a pulse, since the condition $M_{|m|} = (u^2+v^2+M_z^2)^{\frac{1}{2}}$, in the absence of attenuation, does not apply here.

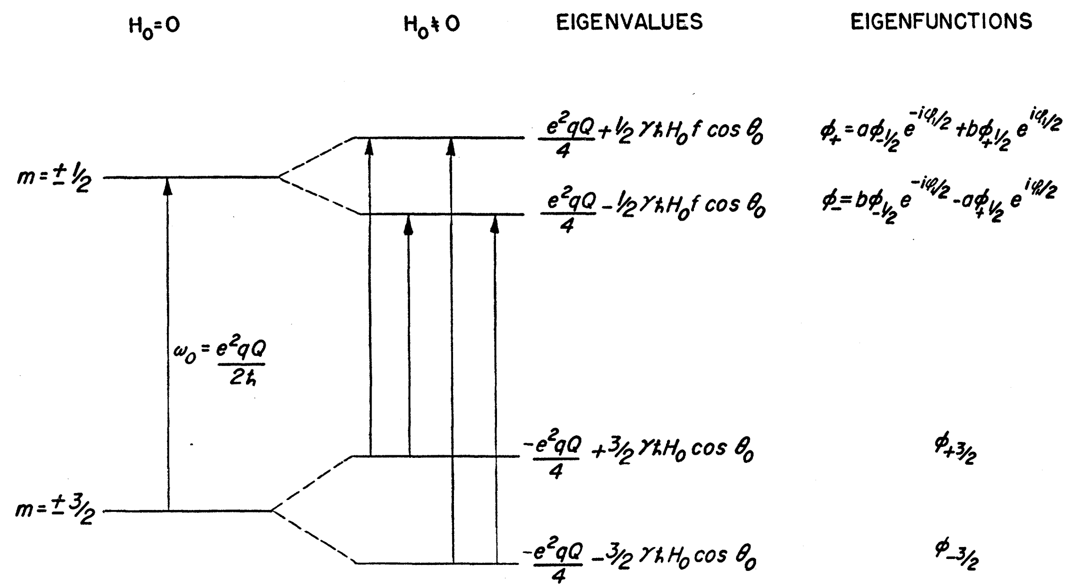

FIG. 2. Energy level diagram for spin $I=\frac{3}{2}$ quadrupole interaction in small magnetic field H_0. A system of coordinates is chosen in which the azimuthal coordinate φ_1 for H_1 is zero. The parameters are
$a=[(f-1)/(2f)]^{\frac{1}{2}}$, $b=[(f+1)/(2f)]^{\frac{1}{2}}$, and $f=(1+4\tan^2\theta_0)^{\frac{1}{2}}$.

For $(E_{|m|}-E_{|m|-1})/kT\ll 1$, Boltzmann statistics gives $M_0=(E_{|m|}-E_{|m|-1})N\gamma\hbar/[2kT(2I+1)]$, where $E_{|m|}-E_{|m|-1}=\frac{3}{4}e^2qQ(2|m|-1)/[I(2I-1)]$. The net macroscopic magnetization $M_z=\gamma\hbar N[|C_{|m|}(t)|^2-|C_{|m|-1}(t)|^2]/2$ is an apparent moment which is the analog of the M_z normally considered in a purely magnetically coupled nuclear induction system. After the single pulse which gave M_x in (25) for a given $|m|$, then

$$M_z=M_0\cos[(I+|m|)^{\frac{1}{2}}(I-|m|+1)^{\frac{1}{2}}\omega_1 t_w], \qquad (26)$$

which implies that M_z can reverse sign if the cosine becomes negative. Physically, of course, the actual magnetism due to superposition of a pair of $|m|$ and $|m|-1$ states can never reverse sign because of the constraint of the quadrupole coupling acting on the nuclear charge distribution. A physical picture of the change in the z component of magnetism for a given sign of m is obtained by evaluating the actual magnetism $\gamma\hbar N\bar{I}_z=M_T$ directly, where $\bar{I}_z$ from (19) is the expectation value. During the application of a single pulse the $a_{|m|,|m|-1}$ coefficients can be obtained from (18) and substituted into (19), which gives

$$M_T=\gamma\hbar N\{|C_{|m|}(0)|^2+|C_{|m|-1}(0)|^2 \qquad (27\text{-A})$$
$$+\tfrac{1}{2}[|C_{|m|}(0)|^2-|C_{|m|-1}(0)|^2]$$
$$\times\cos[(I+|m|)^{\frac{1}{2}}(I-|m|+1)^{\frac{1}{2}}\omega_1 t_w]\}. \qquad (27\text{-B})$$

The term (27-B) corresponds to M_z in (26); let (27-A) be represented by M_k. The M_z change in magnetism would appear along the z axis in an experiment where a circularly polarized rf field H_1 is applied to excite m states of one sign only. Similarly, M_y could then be observed. This procedure would be necessary in order to prevent the cancellation of M_x and M_y by equal and opposite values produced in our experiment, where two circularly polarized components of H_1 are rotating in opposite directions. Figure 1 illustrates the motion of the separate vectors $\mathbf{M}_{+|m|}$ and $\mathbf{M}_{-|m|}$ [however, $M_{|m|}\neq(u^2+v^2+M_z^2)^{\frac{1}{2}}$] corresponding to each sign of m, which are superimposed upon the constant amounts of magnetism M_k.

If a small magnetic field H_0 is applied to the spins along the z axis for example, such that $\gamma\hbar H_0\ll e^2qQ$, the entire vector diagram can be thought of as precessing about H_0 in a direction determined by the sign of γ. Therefore the symmetry of alignment about the x axis of $M_{+|m|}$ and $M_{-|m|}$ is removed, which in essence means that the degeneracy of the $\pm m$ states is removed. A low-frequency modulated induction signal will then appear along the y axis as well as the x axis due to the additional precession imposed by H_0. The next section presents an analysis of this case.

B. Small Magnetic Field Case

First a single rf pulse is applied with conditions imposed as in case A for $I=\frac{3}{2}$ in zero field, with the additional requirement that the conditions γH_1, $1/t_w\gg H_0$ apply. These conditions can be satisfied approximately in the experiment for values of $H_0\lesssim 20$ gauss, and imply that H_0 can be neglected during the application of the pulse since the spin system scarcely precesses because of H_0 during the time t_w. The general Hamiltonian now is

$$\mathcal{H}=-\mathbf{Q}\cdot\nabla\mathbf{E}-\gamma\hbar\mathbf{I}\cdot[\mathbf{H}_0+\mathbf{H}(t)], \qquad (28)$$

where $\mathbf{H}(t)$ is chosen as before, and $\mathbf{H}_0$ is the applied constant field, The directions of H_0 and H_1 in the coordinate system having the symmetry axis of $\nabla\mathbf{E}$ as the z axis are defined by the angles θ_0, φ_0 and θ_1, φ_1 respectively. The matrix of the square bracket may be written in terms of the eigenfunctions of I_z, where the only important off-diagonal terms to first order are those connecting the $m=\pm\frac{1}{2}$ states for $e^2qQ\gg\gamma\hbar H_0$. Diagonalization of the matrix yields the eigenstates and eigenvalues shown in Fig. 2.[13,14] The effect of the magnetic field is not only to remove the degeneracy of the $\pm m$ states, but to mix the $m=\pm\frac{1}{2}$ states, and yet leave all other m states pure. Thus all transitions other than $|m|=\frac{1}{2}\rightleftarrows|m|=\frac{3}{2}$ are similar to the case of $I=\frac{3}{2}$ with H_0 applied in the z direction.

The solution of the Schrödinger equation in the absence of H_1 is then given by

$$\begin{aligned}\psi=&C_{\frac{3}{2}}(t_i)\phi_{\frac{3}{2}}\exp[-i(\omega_{\frac{3}{2}}+\tfrac{3}{2}\Omega_0\cos\theta_0)(t-t_i)]\\&+C_{-\frac{3}{2}}(t_i)\phi_{-\frac{3}{2}}\exp[-i(\omega_{\frac{3}{2}}-\tfrac{3}{2}\Omega_0\cos\theta_0)(t-t_i)]\\&+C_{+}(t_i)\phi_{+}\exp[-i(\omega_{\frac{1}{2}}+\tfrac{1}{2}f\Omega_0\cos\theta_0)(t-t_i)]\\&+C_{-}(t_i)\phi_{-}\exp[-i(\omega_{\frac{1}{2}}-\tfrac{1}{2}f\Omega_0\cos\theta_0)(t-t_i)],\end{aligned}\quad(29)$$

where $\Omega_0=\gamma H_0$ and $C_{\frac{3}{2}}(t_i)$, $C_{-\frac{3}{2}}(t_i)$, $C_+(t_i)$, and $C_-(t_i)$ are population coefficients determined from initial conditions at $t_i=t_w$ following the rf pulse. The coefficients $C_{\frac{3}{2}}(t_w)$ and $C_{-\frac{3}{2}}(t_w)$ are obtained directly from Eq. (10) in Sec. II-A, whereas $C_+(t_w)$ and $C_-(t_w)$ are determined from relations which equate coefficients $C_{\pm\frac{1}{2}}(t_w)$ in (10) to the collected coefficients of $\phi_{\pm\frac{1}{2}}$ in (29) when $t_i=t_w$. The expectation value of I_+ is then computed, as before, to describe the free precession after the pulse, now using ψ in Eq. (29). A lengthy expression is obtained, which we will not reproduce here. Low-frequency terms involving Ω_0 appear which may be neglected because they produce a negligible induction effect for $\Omega_0\ll\omega_0$. The induction voltage developed across the coil is proportional to $\bar{I}_x$. The observed macroscopic moment $\gamma\hbar N\bar{I}_x$ for $t\geqslant t_w$ is given by

$$\begin{aligned}\mathfrak{M}_x=&2\sqrt{3}M_0\sin\theta_1\sin\omega_0t\sin(\sqrt{3}\omega_1t_w\sin\theta_1)\\&\times\left\{\left(\frac{f+1}{2f}\right)\cos\left[\Omega_0(\cos\theta_0)(3-f)\frac{t}{2}\right]\right.\\&\left.+\left(\frac{f-1}{2f}\right)\cos\left[\Omega_0(\cos\theta_0)(3+f)\frac{t}{2}\right]\right\},\end{aligned}\quad(30)$$

with no decay effects included. A similar expression is obtained for M_y. H_1 is chosen here in the experiment to be perpendicular to H_0. Now in addition to the fact that a spread in the field gradient eq causes a decay of M_x, a spread in H_0 due either to external field inhomogeneities or to local magnetic dipole fields of nuclear neighbors will likewise cause a static distribution of induction frequencies in the crystal, given by

$$g(\Omega_0'-\Omega_0)=[\exp-(\Omega_0'-\Omega_0)^2/(2\eta^2)]/(2\pi\eta^2)^{\frac{1}{2}}.\quad(31)$$

This distribution function, similar to (14), can be assumed for the distribution in H_0, particularly if it is due to nuclear neighbors, where η is the root mean square deviation of frequency due to internal dipolar magnetic fields. The average of (30) over both the distribution functions (14) and (31), where we let $\omega_0\to\omega_0+(\omega_0'-\omega_0)$ and $\Omega_0\to\Omega_0+(\Omega_0'-\Omega_0)$ in (30), is

$$\begin{aligned}\langle\mathfrak{M}_x\rangle_{\text{Av}}=&2\sqrt{3}M_0\sin\theta_1\sin\omega_0t\sin(\sqrt{3}\omega_1t_w\sin\theta_1)\\&\times\exp(-\delta^2t^2/2)\\&\times\left\{\left(\frac{f+1}{2f}\right)\cos[\Omega_0(\cos\theta_0)(3-f)t/2]\right.\\&\times\exp[-\eta^2(\cos^2\theta_0)(3-f)^2t^2/8]\\&+\left(\frac{f-1}{2f}\right)\cos[\Omega_0(\cos\theta_0)(3+f)t/2]\\&\left.\times\exp[-\eta^2(\cos^2\theta_0)(3+f)^2t^2/8]\right\}.\end{aligned}\quad(32)$$

Of course, the angle θ_0 for the internal field at different nuclear sites is random in direction, but we choose here not to average over this angle, which must be done to describe the actual decay. We assume in (32) that η is the equivalent of an average internal field which lies along the direction of the externally applied H_0 and is independent of θ_0. It should also be kept in mind that our discussion here does not include any decay due to T_1 or to effects which involve time dependent fluctuations of the local dipolar fields, both of which are to be treated in later papers. The magnetization component therefore predicts an induction signal modulated by two different frequencies which are associated with the splitting of the original quadrupole resonance into lines symmetrically distributed relative to the original line (see Fig. 2).

C. The Quadrupole Spin Echo in Small Field

In addition to the first rf pulse applied in the above case, let a second pulse be turned at $t=\tau$ and turned off at $t=\tau+t_w$. The initial spin population coefficients for the second pulse at $t=\tau$ are obtained from Eq. (29). The solution of the Schrödinger equation then provides new population coefficients at $t=\tau+t_w$ which are matched to the free precession solution during the time $t\geqslant\tau+t_w$. The induction without decay for $t\geqslant\tau+t_w$

[13] B. T. Feld and W. E. Lamb, Phys. Rev. **67**, 28 (1945).
[14] C. Dean, thesis, Harvard University, 1952 (unpublished) and Phys. Rev. **96**, 1053 (1954).

is then found to be

$$\mathfrak{M}_x=-2\sqrt{3}M_0\sin\theta_1\Bigg[\sin(\omega_1t_w)\cos^2\left(\frac{\omega_1t_w}{2}\right)\left\{\left(\frac{f+1}{2f}\right)\cos[\Omega_0(\cos\theta_0)(3-f)t/2]+\left(\frac{f-1}{2f}\right)\cos[\Omega_0(\cos\theta_0)(3+f)t/2]\right\}\sin\omega_0t \quad \text{(33-I)}$$

$$-\tfrac{1}{2}\sin(2\omega_1t_w)\left\{\left(\frac{f+1}{2f}\right)\cos[\Omega_0(\cos\theta_0)(3-f)(t-\tau)/2]+\left(\frac{f-1}{2f}\right)\cos[\Omega_0(\cos\theta_0)(3+f)(t-\tau)/2]\right\}\sin\omega_0(t-\tau) \quad \text{(33-II)}$$

$$+\sin(\omega_1t_w)\sin^2\left(\frac{\omega_1t_w}{2}\right)\left\{\left(\frac{f+1}{2f}\right)^2\cos[\Omega_0(\cos\theta_0)(3-f)(t-2\tau)/2]+\left(\frac{f-1}{2f}\right)^2\cos[\Omega_0(\cos\theta_0)(3+f)(t-2\tau)/2]\right\}\sin\omega_0(t-2\tau) \quad \text{(33-III)}$$

$$+\sin(\omega_1t_w)\sin^2\left(\frac{\omega_1t_w}{2}\right)\left(\frac{f^2-1}{2f^2}\right)\Big\{\cos[3\Omega_0(\cos\theta_0)t/2]\cos[f\Omega_0(\cos\theta_0)(t-2\tau)/2]+\cos[3\Omega_0(\cos\theta_0)(t-2\tau)/2]$$
$$\times\cos[f\Omega_0(\cos\theta_0)t/2]-\cos[3\Omega(\cos\theta_0)t/2]\cos[f\Omega_0(\cos\theta_0)t/2]\Big\}\sin\omega_0(t-2\tau)\Bigg]. \quad \text{(33-IV)}$$

A similar expression is obtained for $\mathfrak{M}_y$. In order to interpret the various terms as they contribute to the observed signals, it is essential that each term in (33) be averaged over the assumed static Gaussian distributions in eq and Ω_0 given by (14) and (31) respectively. Equation (32) indicates the result of such an averaging after the first pulse. Each of the terms in (33) becomes multiplied by a Gaussian decay factor $\exp(-\alpha\eta^2t_1^2/2-\delta^2t_2^2/2)$ where α depends upon factors in the cosine arguments involving Ω_0, and t_1 is the time factor which accompanies them. The time t_2 pertains to the particular time factor in the sine function which is averaged over $\omega_0'-\omega_0$. Term I, which is due to a remnant of the free precession following the first pulse, is usually not observed after the second pulse and in fact is avoided by making τ sufficiently large. Term II is the free precession tail which follows after the second pulse if the average magnetization $\bar{M}_z(t_w)$ happens to be nonzero after application of the first pulse. $\bar{M}_z(\tau)$ can also be nonzero due to thermal relaxation of nuclei excited by the first pulse. The latter effect is not included here since we have assumed T_1 to be infinite, and hence $M_z(t_w)=M_z(\tau)$. An extra term omitted here describes a signal that can be utilized to measure T_1 (see reference 6). The measurement of T_1 in some quadrupole systems will be described by one of us (M.B.) in a later paper. Term III is the "normal" spin echo at $t=2\tau$ which has a maximum amplitude independent of the static spread in precessional frequencies throughout the crystal. Term IV is an additional contribution to the spin echo signal discussed previously by Bloom,[15] which has a periodic amplitude as a function of τ, and so gives rise to a slow echo envelope beat with a period $\sim 2\pi/\Omega_0$. The contribution from this term, however, attenuates rapidly in a time of the order of $2\pi/\eta$. The slow beats here provide an interesting analog to the echo envelope modulation slow beats previously observed in nuclear magnetic resonance[9,16] for resonances exhibiting multiplet structure due to the indirect nuclear spin-spin coupling. In that interaction between identical but chemically nonequivalent nuclei, mixtures of singlet and triplet spin states bring about an interference between spin states which is manifested by the slow echo beats. For quadrupole echoes the mixing of the $m=\pm\frac{1}{2}$ states due to the Zeeman effect gives rise to the slow beats for the same reason. Note that the slow-beat Term IV vanishes for $\theta=0$ or π ($f\to 1$), corresponding to the condition that H_0 does not mix the $m=\pm\frac{1}{2}$ states so that they form two independent systems. This is analogous to the fact that there are no slow beats in the case of identical nuclei in the earlier magnetic resonance experiments, where two groups of like nuclei have different chemical shifts but have a zero indirect spin-spin interaction.

III. CHLORINE FREE INDUCTION SIGNALS FROM $NaClO_3$

The quadrupole coupling of chlorine in $NaClO_3$ is a standard case which has been studied by several observers.[17] The electric field gradient eq is assumed to be axially symmetric about the molecular bond (z axis) joining Na to Cl. Figure 3 shows the $NaClO_3$ unit cell, which has four chlorine nuclei with their axes of quan-

[15] M. Bloom, Phys. Rev. 94, 1396 (1954).

[16] McNeil, Slichter, and Gutowsky, Phys. Rev. 84, 1245 (1951).

[17] Wang, Townes, Schawlow, and Holden, Phys. Rev. 86, 809 (1952); R. Livingston, Science 118, 61 (1953); J. Itoh and R. Kusaka, J. Phys. Soc. Japan 9, 434 (1954); Ting, Manring, and Williams, Phys. Rev. 96, 408 (1954).

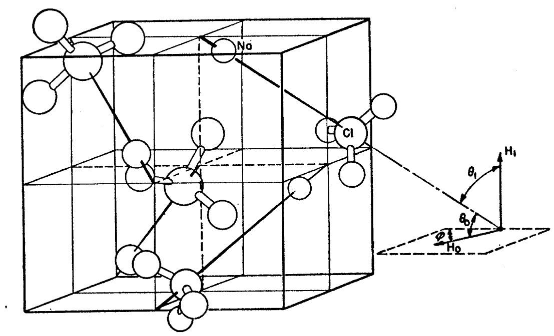

FIG. 3. Crystal structure of $NaClO_3$. The cubic lattice unit cell dimension is 6.57 A on a side.

tization oriented along the body diagonals of the subcubic cells. There are two nonequivalent directions of Na−Cl axes with respect to H_0, and a pair of chlorine nuclei assigned to each of these directions is denoted by $+$ and $-$. The shapes of free precession signals due to the Cl^{35} nucleus serve to confirm the expressions obtained in Eqs. (32) and (33-III). Specific cases are shown in Fig. 4, where an external H_0 field is perpendicular to the cubic axis of symmetry and the rf field $2H_1$ is perpendicular to H_0.

The lifetime of free precession following a pulse is determined primarily by magnetic dipolar broadening due to nearest sodium neighbors, which provide a root mean square local field $h_0=0.80$ gauss at chlorine sites. In order to determine η in (31), which is the effective mean square local field, the effect of h_0 on each of the quadrupole m states must be evaluated, which requires a knowledge of the net parallel and perpendicular components of h_0 with respect to the Na−Cl axis. Such a calculation yields $T_2^*=0.48$ millisecond, assuming that $T_2^{*2}=1/\eta^2$. The observed T_2^* is shorter ($\sim$0.3 millisecond), because of possible temperature gradients, strains in the crystal, Zeeman broadening due to the earth's field (particularly in powdered samples), and because of the additional but smaller broadening due to coupling among chlorine nuclei. The thermal relaxation time T_1 scarcely affects the observed relaxation here, since $T_1\sim 23$ milliseconds at room temperature. The observed signal following the first pulse is given by $V=V_+ + V_-$, where

$$V_\pm = 2\sqrt{3}M_0(\cos\theta_\pm)\sin(\sqrt{3}\omega_1 t_w\cos\theta_\pm)\times\left\{\left(\frac{\beta_\pm-1}{\beta_\pm}\right)\cos[\Omega_0(\cos\theta_\pm)(3+\beta_\pm)t/2]+\left(\frac{\beta_\pm+1}{\beta_\pm}\right)\cos[\Omega_0(\cos\theta_\pm)(3-\beta_\pm)t/2]\right\}\times\exp(-t^2/2T_2^{*2}), \quad (34)$$

and the echo signal[18] (for $t\gg 1-\eta$) is described by

$$V_\pm = -2\sqrt{3}M_0(\cos\theta_\pm)\sin(\sqrt{3}\omega_1 t_w\cos\theta_\pm)\times\sin^2[\sqrt{3}\omega_1 t_w(\cos\theta_\pm)/2]\left\{\left(\frac{\beta_\pm-1}{\beta_\pm}\right)^2\times\cos[\Omega_0(\cos\theta_\pm)(3+\beta_\pm)(t-2\tau)/2]+\left(\frac{\beta_\pm+1}{\beta_\pm}\right)^2\cos[\Omega_0(\cos\theta_\pm)(3-\beta_\pm)(t-2\tau)/2]\right\}\times\exp-[(t-2\tau)^2/2T_2^{*2}+t^2/T_2'^2(H_0,\varphi)]. \quad (35)$$

In terms of the angle φ which H_0 makes with respect to the 100 direction in $NaClO_3$, $\cos\theta_\pm=\sqrt{\tfrac{2}{3}}\cos(\varphi\pm\tfrac{1}{4}\pi)$ and $\sin\theta_\pm=[1-\tfrac{2}{3}\cos^2(\varphi\pm\tfrac{1}{4}\pi)]^{\frac{1}{2}}$, where θ is the angle H_0 makes with the Na−Cl bond. Also

$$\beta_\pm=(1+4\tan^2\theta_\pm)^{\frac{1}{2}}.$$

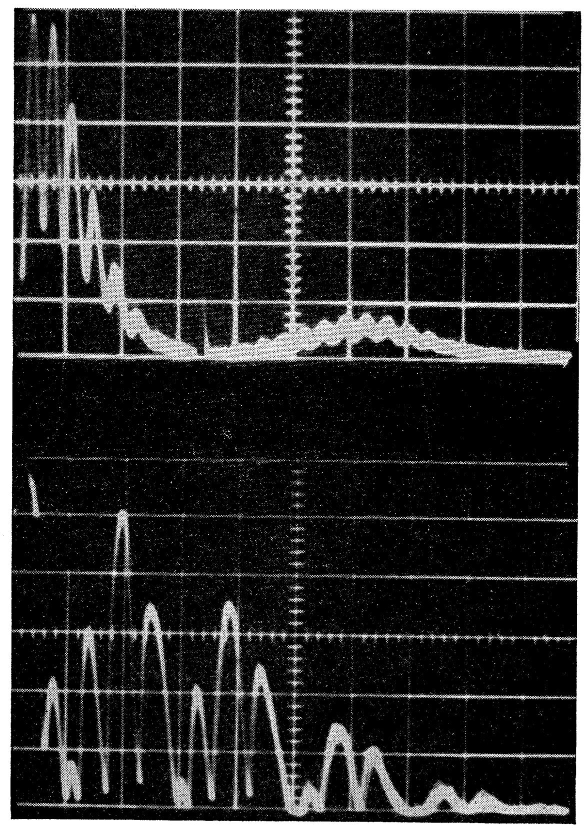

FIG. 4. Oscillographic display of free precession signals due to Cl^{35} in a single $NaClO_3$ crystal in the presence of a small magnetic field H_0. The upper trace shows free precession following a first pulse, and an echo at $t=2\tau$ after a second pulse applied at $t=\tau$, where $\sqrt{3}\omega_1 t_w=\pi/2$ for both pulses. A magnetic field of $H_0=11.4$ gauss is applied along the crystalline 1, 0, 0 direction ($\varphi=0$). The signal shapes are described by Eqs. (34) and (35). The sweep length is 2.5 milliseconds. The lower trace illustrates the free precession following a single pulse for $H_0=25$ gauss along the crystalline $1/\sqrt{2}$, $1/\sqrt{2}$, 0 direction ($\varphi=45°$). From Eq. (34) the signal shape, excluding attenuation, is given by

$$V(t)\propto 0.4\cos(1.9\Omega_0 t)+1.6\cos(0.53\Omega_0 t)+2\cos(\Omega_0 t).$$

The sweep length is one millisecond.

[18] In reference 2, the square superscript was omitted in error for the coefficients involving $\beta_\pm$.

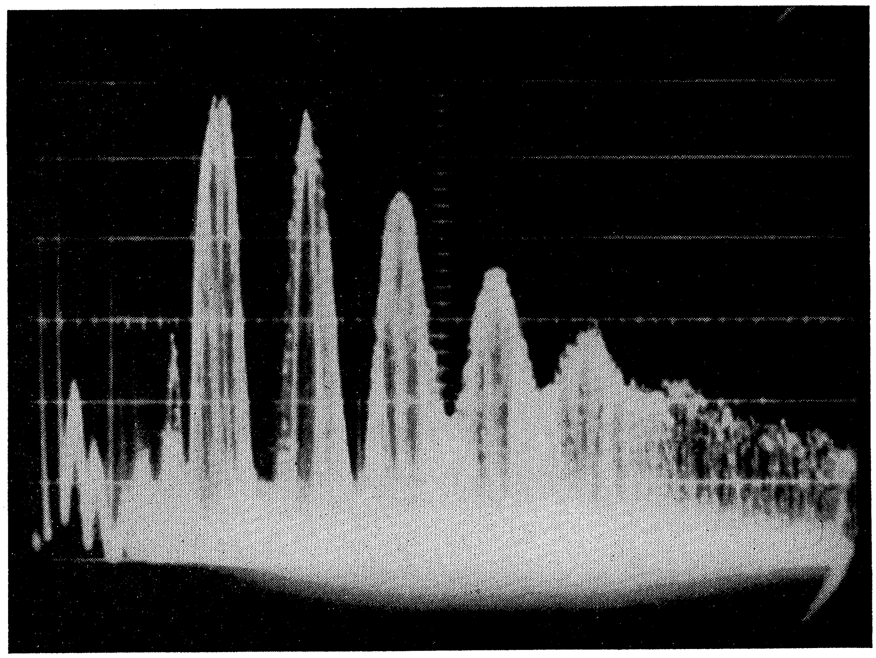

FIG. 5. Echo envelope trace of slow beat modulation due to Cl^{35} in a single $NaClO_3$ crystal. $H_0=11.8$ gauss in the crystalline 1,0,0 direction ($\varphi=0$). The sweep length is 2.0 milliseconds.

The static contribution to the relaxation time is in terms of $T_2^{*2}\cong 1/(\eta^2+\delta^2)$, and the dynamic contribution to the relaxation which excludes the effect of T_1, but includes the effect of time varying local fields and spin-spin coupling, is lumped together in terms of $T_2'^2$. For each setting of τ, with the spin ensemble at thermal equilibrium, the maximum of the echo amplitude is observed to be proportional to $\exp[-(2\tau)^2/T_2'^2(H_0,\varphi)]$. The time constant T_2' is observed to be a function of φ and H_0. The principal cause for this effect[2] in $NaClO_3$ will be shown in some detail in a later paper by two of us (E.L.H. and B.H.) to be the fact that the spin-spin coupling among the Na nuclei is modified considerably by the Zeeman splitting. A similar but weaker effect occurs due to coupling among Cl nuclei. The correlation time of local fields at Cl sites, due to the spin-spin coupling among Na dipoles, is therefore modified and a change in T_2' is observed.

Figure 5 illustrates the slow beats in $NaClO_3$. An artificial distribution of eq is imposed by introducing a temperature gradient across the sample. Otherwise the free induction signal due to the signal (32) following the first pulse would interfere with echoes exhibiting the echo slow beat, which only lasts for a time $2\tau\sim 2\pi/\eta$. This is also approximately the natural lifetime of the free induction tail. The lifetime of the echo is relatively unaffected by a gradient in eq. Hence the echo remains visible whereas the induction signal is now sufficiently attenuated due to decay factor involving $\delta(\delta\gg\eta)$ and does not interfere with the echo. Now terms (33-III) and (33-IV) are applied to the case of $NaClO_3$, and contributions from the two nonequivalent positions of Cl in the unit cell must be added. For the case where H_0 is oriented along the 1,0,0 axis, the echo envelope slow beat, including only the decay due to dipolar broadening, is predicted to be

$$V(2\tau)\propto(5/9)+(8/9)\cos(\sqrt{3}\Omega_0\tau)\exp(-3\eta^2\tau^2/2)$$
$$+(2/9)[1+\cos(2\sqrt{3}\Omega_0\tau)]\exp(-6\eta^2\tau^2)],$$

which is confirmed by Fig. 4. Other orientations of H_0 give a more complicated pattern. The slow beats are also observed in a crystalline powder, where the beat structure also persists for a time $\sim 2\pi/\eta$, even though the electric field gradients are oriented in random directions with respect to H_0.

IV. APPARATUS

The apparatus for production and detection of quadrupole free precession signals is similar to that used

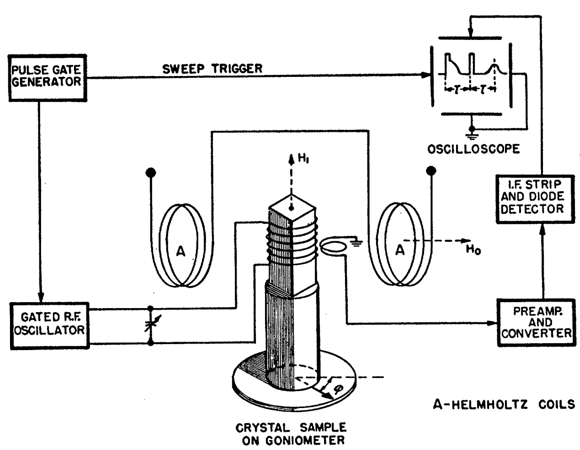

FIG. 6. Block diagram of apparatus for obtaining nuclear quadrupole free precession.

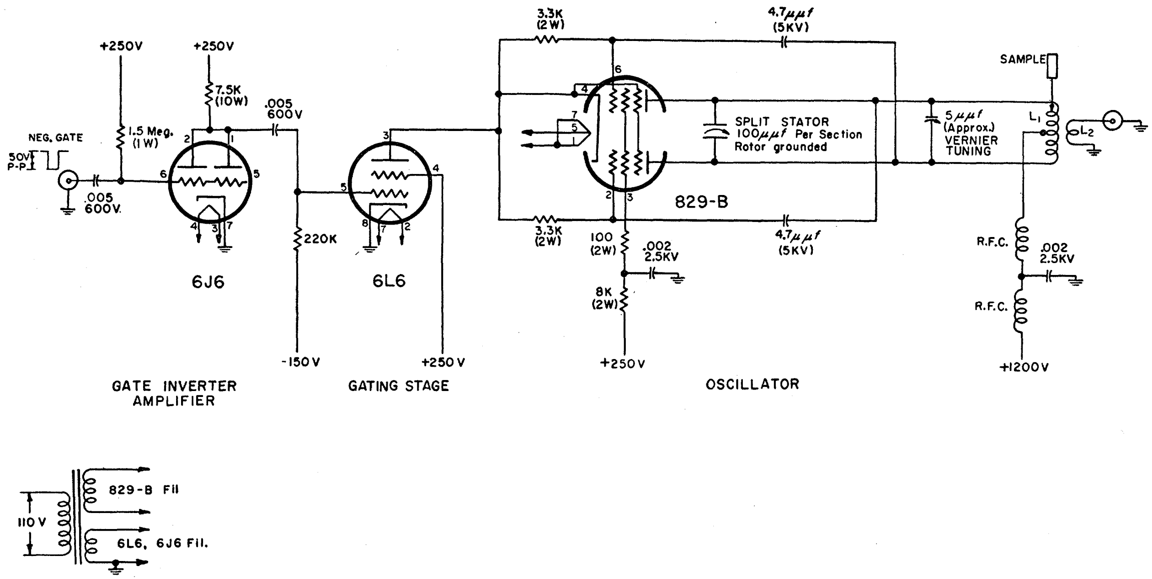

FIG. 7. 30 Mc/sec pulsed oscillator for obtaining free nuclear quadrupole precession.

previously in observing spin echoes in nuclear magnetic resonance. When zero-field quadrupole signals are to be observed, however, it is essential that the receiving coil be coaxial with the transmitting coil—the transmitting coil may actually serve as the receiving coil—for reasons discussed previously. A block diagram, Fig. 6, shows the apparatus used. The transmitter (circuit diagram in Fig. 7) consists of a pulsed oscillator normally held at cutoff and brought into oscillation by negative gating pulses. The gating unit triggers the oscilloscope sweep and, after suitable delay, provides several negative gates of equal but variable width and variable time separations.

In free precession experiments the two receiver problems are: (1) adequately short recovery time of receiver sensitivity following intense transmitter pulses to allow observation of induction signals of short lifetime; (2) sufficient signal to noise ratio for reception of weak nuclear signals. Experience has shown that a tuned rf receiver consisting of a low noise preamplifier followed by a broadband radar i.f. strip with crystal detector suffices for experiments carried out in the

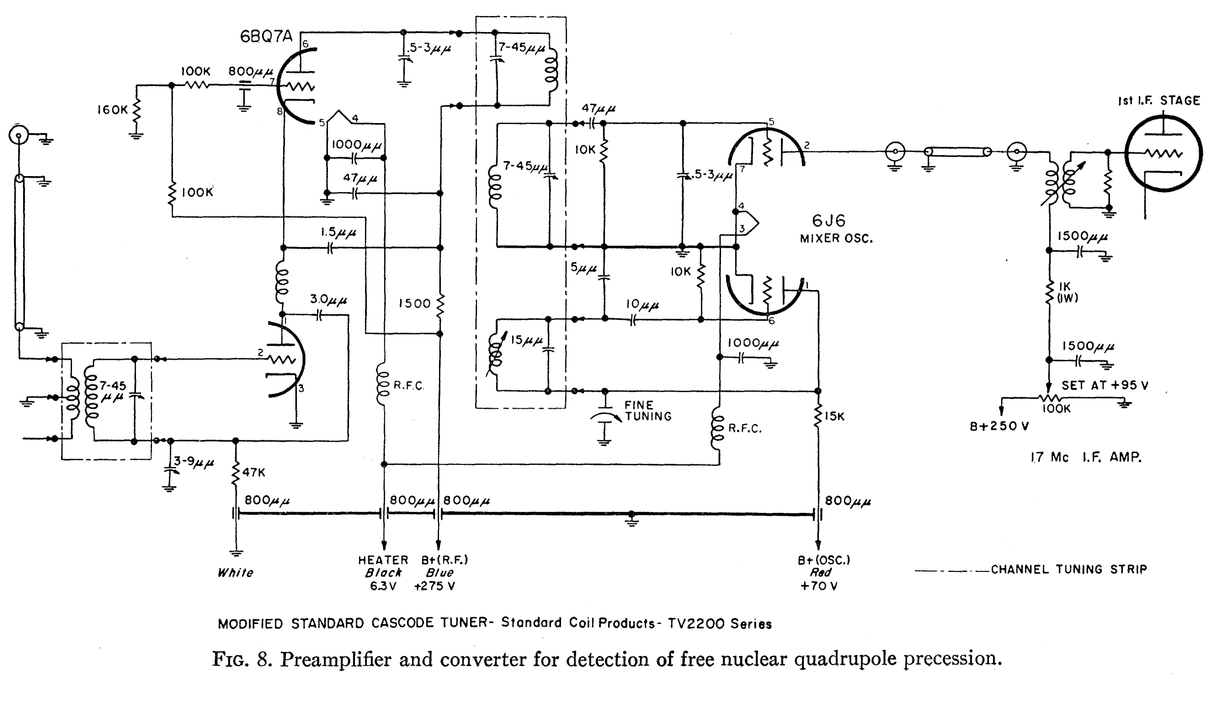

FIG. 8. Preamplifier and converter for detection of free nuclear quadrupole precession.

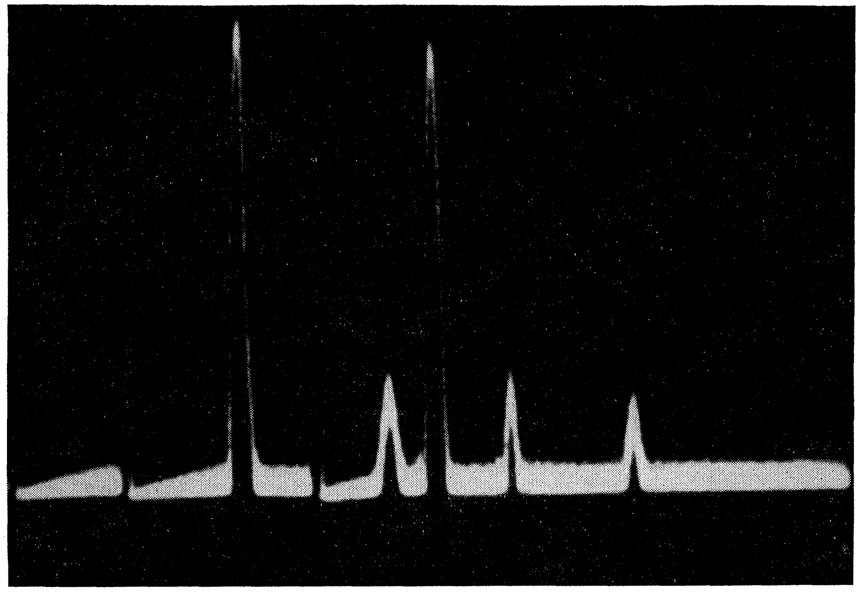

FIG. 9. Oscillographic display of spin echo signals at 150 mc from Br^{81} in powdered $NaBrO_3$ due to the application of three rf pulses at $t=0$, $t=\tau$, and $t=T$. The sweep length is 2 milliseconds, $\tau=0.27$ millisecond, and $T=0.71$ millisecond. A magnetic field of $H_0=10$ gauss is applied to enhance the echo signals (see reference 2).

region of 30 Mc/sec, and has adequate recovery time. However, the problems of instability and of tuning, as well as the difficulty of adapting the tuned rf system to higher resonant frequencies, such as the 150 Mc/sec resonance of Br^{81} in $NaBrO_3$, has led to the use of a modified television superheterodyne tuner.

Figure 8 shows such a converter modified for quadrupole resonance detection in the 30 Mc/sec region. The initial 6 Mc/sec band pass of the television tuner was reduced by removing the damping resistor across the input coil. The input, oscillator, and mixer coils (mounted on a plastic bar "channel tuning strip") were trimmed to the desired frequency with condensers. To reduce recovery time of the mixer input, a "rf test point" (indicated on the commercial tuner) below the $10K$ resistor in the grid circuit was grounded. For best signal to noise ratio adjustment, separate B^+ supplies for local oscillator and mixer were provided. The mixer output coil was placed directly in the 17 Mc/sec i.f. strip to simplify tuning. The receiver has a sensitivity of $\sim$1.0 microvolts for a signal to noise ratio of unity, and a recovery time of $\sim$20 microseconds when intense rf pulses are applied to the input.

V. CONCLUDING REMARKS

An initial study has been presented of transient nuclear induction in systems of quadrupole moments in which nuclear polarization and precession is principally determined by nuclear quadrupole coupling to an axial electric field gradient. Various effects pertaining to nuclear relaxation times and crystal structure studies by means of Zeeman structure analysis remain to be investigated in many crystals. The pulsed spin echo method lends itself particularly to a clear-cut means of separating the various contributions to spin relaxation: (*a*) thermal spin relaxation times T_1; (*b*) static spread in the line width in terms of a transient induction decay; and (*c*) dynamic fluctuations of local fields in the lattice causing echo envelope decay. A study of these various contributions as they are influenced by changes in parameters such as temperature and pressure and, for example, the relaxation behavior under the influence of acoustic vibrations should yield interesting results. The method of double nuclear resonance can be applied to nuclear quadrupole free induction studies to reveal new information regarding nuclear spin coupling[19] and relaxation. Cases in free precession remain to be studied in which the electric field gradient is assymetric. The effect of the asymmetry upon the beats due to the Zeeman effect should be of interest.

Two of us (E.L.H. and B.H.) wish to thank Mr. Blume, Mr. Jones, and Mr. Kiselewsky for their excellent work and assistance in the construction of the apparatus. We thank Dr. T. Wang for discussions and Dr. A. Schawlow of Bell Laboratories for provision of an $NaClO_3$ single crystal. Miss Alice Waara helped in preparing the drawings. One of us (M.B.) wishes to thank Professor C. P. Slichter and Professor R. E. Norberg for many valuable discussions.

[19] B. Herzog and E. L. Hahn, Bull. Am. Phys. Soc. **29**, No. 7, 11 (1954); E. L. Hahn and B. Herzog, Bull. Am. Phys. Soc. **29**, No. 8, 17 (1954).

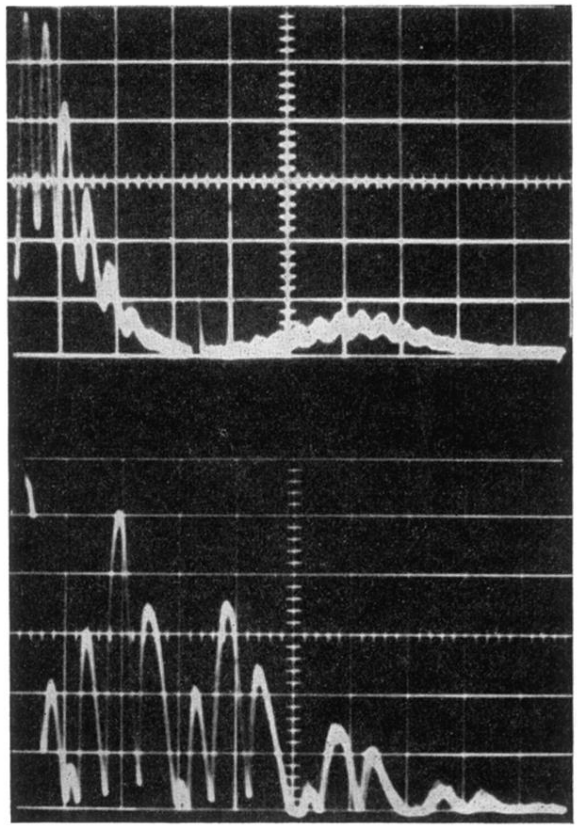

FIG. 4. Oscillographic display of free precession signals due to Cl^{35} in a single $NaClO_3$ crystal in the presence of a small magnetic field H_0. The upper trace shows free precession following a first pulse, and an echo at $t=2\tau$ after a second pulse applied at $t=\tau$, where $\sqrt{3}\omega_1 t_w=\pi/2$ for both pulses. A magnetic field of $H_0=11.4$ gauss is applied along the crystalline 1, 0, 0 direction ($\varphi=0$). The signal shapes are described by Eqs. (34) and (35). The sweep length is 2.5 milliseconds. The lower trace illustrates the free precession following a single pulse for $H_0=25$ gauss along the crystalline $1/\sqrt{2}$, $1/\sqrt{2}$, 0 direction ($\varphi=45°$). From Eq. (34) the signal shape, excluding attenuation, is given by

$$V(t) \propto 0.4 \cos(1.9\Omega_0 t)+1.6 \cos(0.53\Omega_0 t)+2 \cos(\Omega_0 t).$$

The sweep length is one millisecond.

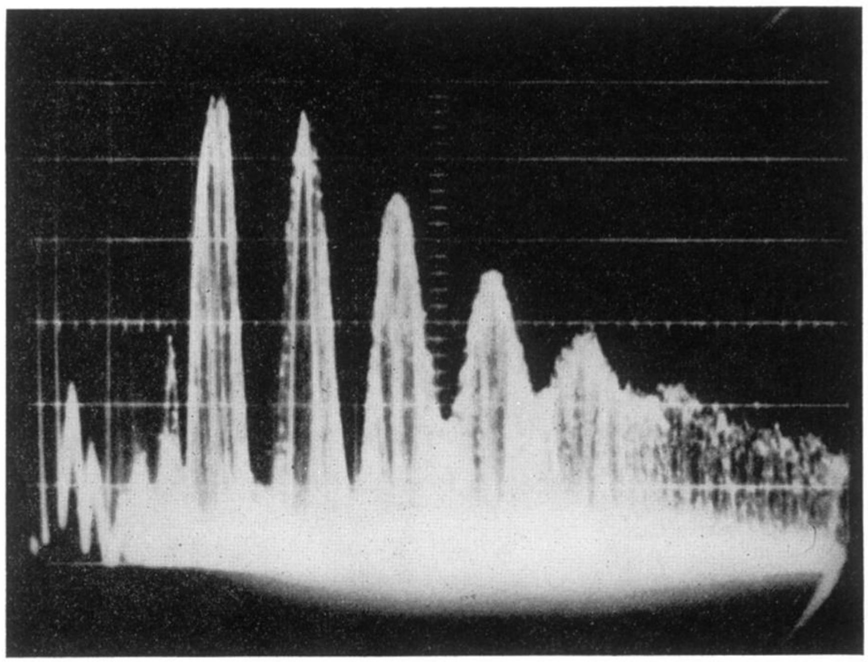

FIG. 5. Echo envelope trace of slow beat modulation due to Cl^{35} in a single $NaClO_3$ crystal. $H_0 = 11.8$ gauss in the crystalline 1,0,0 direction ($\varphi = 0$). The sweep length is 2.0 milliseconds.

FIG. 9. Oscillographic display of spin echo signals at 150 mc from Br^{81} in powdered $NaBrO_3$ due to the application of three rf pulses at $t=0$, $t=\tau$, and $t=T$. The sweep length is 2 milliseconds, $\tau=0.27$ millisecond, and $T=0.71$ millisecond. A magnetic field of $H_0=10$ gauss is applied to enhance the echo signals (see reference 2).